

Primljen / Received: 28.10.2023.

Ispravljen / Corrected: 21.6.2024.

Prihvaćen / Accepted: 27.8.2024.

Dostupno online / Available online: 10.9.2024.

# Numerical modelling of masonry structural joint repointing: finite element analysis based on experimental investigations

## Authors:

Prof. **Sergey Churilov**, PhD. CE

University of St. Cyril and Methodius in Skopje

Faculty of Civil Engineering

[curilov@gf.ukim.edu.mk](mailto:curilov@gf.ukim.edu.mk)

Corresponding author

Prof. **Elena Dumova-Jovanoska**, PhD. CE

University of St. Cyril and Methodius in Skopje

Faculty of Civil Engineering

[dumova@gf.ukim.edu.mk](mailto:dumova@gf.ukim.edu.mk)

Research Paper

**Sergey Churilov, Elena Dumova-Jovanoska**

## Numerical modelling of masonry structural joint repointing: finite element analysis based on experimental investigations

This study investigated the efficacy of joint repointing as a strengthening technique for unreinforced masonry (URM) structures via experimental data combined with advanced numerical modelling. The numerical simulations demonstrated remarkable alignment with the experimental data, validating the efficacy of the proposed modelling approach. The finite element analysis results were consistent with the experimentally observed stress–strain relationships, failure modes, and ultimate capacities of the masonry panels. The calibrated model successfully replicated the enhanced performance of the strengthened specimens, particularly in terms of increased compressive and shear strengths. Although parametric studies were not performed directly in this study, the validated numerical model provides a solid foundation for future investigations. The accurate reproduction of experimental results through finite element modelling facilitates the potential for extensive parametric analyses, which could explore various strengthening configurations and material properties without the need for costly and time-consuming physical experiments—particularly valuable for assessing and optimising retrofitting strategies for existing URM buildings, particularly in seismic-prone regions. This research contributes significantly to the field of structural engineering by demonstrating the potential of simplified micromodelling techniques to capture the intricacies of masonry behaviour at the meso-level.

### Key words:

simplified micro-modelling, unreinforced masonry, joint repointing strengthening, nonlinear finite element analysis, masonry interface modelling

Prethodno priopćenje

**Sergey Churilov, Elena Dumova-Jovanoska**

## Numeričko modeliranje reprofiliranja sljubnica ziđa: analiza konačnih elemenata temeljena na eksperimentalnim istraživanjima

U ovom je istraživanju ispitana učinkovitost reprofiliranja sljubnica kao metode pojačanja za zgrade od običnog ziđa na temelju eksperimentalnih podataka u kombinaciji s naprednim numeričkim modeliranjem. Rezultati numeričkih simulacija dokazali su značajnu usklađenost s eksperimentalnim podacima i potvrdili učinkovitost predloženog pristupa modeliranju. Rezultati analize konačnih elemenata bili su u skladu s odnosima naprezanja i deformacija iz eksperimenta, oblicima otkazivanja nosivostima zidanih panela. Kalibrirani model uspješno je ponovio poboljšano ponašanje pojačanih uzoraka, posebno u smislu povećane tlačne i posmične čvrstoće. Iako parametarske analize nisu provedene izravno u ovom istraživanju, provjereni numerički model osigurava čvrsto polazište za buduća istraživanja. Točno reproduciranje eksperimentalnih rezultata pomoću modeliranja na bazi konačnih elemenata omogućuje provođenje opsežnih parametarskih analiza koje bi se mogle upotrijebiti za istraživanje različitih rasporeda pojačanja i svojstava materijala bez potrebe za skupim i dugotrajnim fizičkim eksperimentima. To je osobito korisno za procjenu i optimizaciju metoda obnove za postojeće zgrade od običnog ziđa, osobito u područjima koja su sklona potresima. Ovo istraživanje značajno pridonosi području građevinskih konstrukcija pokazivanjem mogućih pojednostavljenih metoda mikromodeliranja za bilježenje zamršenosti ponašanja ziđa na mezorazini.

### Ključne riječi:

pojednostavljeno mikromodeliranje, obično ziđe, reprofiliranje sljubnica, nelinearna analiza konačnih elemenata, modeliranje interakcija u sljubnicama kod ziđa

## 1. Introduction

Masonry structures have long been a fundamental part of built heritage worldwide. However, the preservation and safety of these structures, particularly under seismic conditions, remain of paramount concern [1-3]. The unpredictable nature of seismic events necessitates advanced analytical tools that can help provide a deeper understanding of masonry behaviour. Computational modelling using numerical simulations is a valuable tool for analysing the behaviour of masonry structures under various loading conditions [4-9], particularly important because many parameters governing the behaviour of the simulated element, part, or structure are not known or cannot be precisely determined by experimental tests. One of the significant advantages of using computational simulations is that they allow the analysis of complex and nonlinear behaviours not easily replicated in laboratory experiments. Accurately modelling the structure and constituent materials can provide valuable insights into the structural behaviour and performance of masonry structures.

Computational modelling can also help design more effective strengthening methods by testing and evaluating different strategies before their implementation in an actual structure [10-14], thus reducing the time and cost associated with physical testing and providing a more accurate assessment of the performance of different repointing methods.

As the most used method for the numerical simulation of masonry structures and materials, the finite element method (FEM) is a versatile method that can handle complex geometries, nonlinear material behaviours, and different loading conditions and can also account for the effects of joints, cracks, and other characteristics of masonry structures [15-22]. However, finite element simulations have limitations. For example, the accuracy of simulations is highly dependent on the accuracy of the input data, such as material properties and loading conditions. In addition, the complexity of the simulations can make them computationally expensive and time-consuming.

Other computational modelling techniques can be used to simulate certain aspects of masonry structures and materials. For example, the discrete element method (DEM) can be used to simulate the behaviour of individual masonry units and their interactions with each other and the mortar [23-28].

Unlike the FEM and DEM, the applied element method (AEM) offers a unique approach that combines the strengths of both methods by discretising structures into small elements connected by springs, allowing for a more detailed simulation of crack initiation and propagation as well as the overall collapse process [29]. Numerical modelling of the seismic behaviour of masonry structures and experimentally tested panels loaded in-plane and out-of-plane offers considerable potential for assessing existing structures and satisfactory agreement between experimental and numerical responses [30-34].

Nevertheless, FEM is considered a powerful tool that enables researchers and engineers to predict and simulate complex

interactions within masonry structures under various load scenarios, including seismic forces, and to replicate experimental results, thereby providing valuable insights into the performance of masonry structures. The reliability of such predictions is essential for making informed decisions regarding structural integrity, retrofitting, and design practices.

Finite element modelling of masonry is important because it facilitates predicting the strength and deformation capacity of retrofitted masonry walls [36]. Masonry structures have poor tensile strength and ductility, making modelling their mechanical behaviour difficult [37]. Traditional finite element analysis faces difficulties in modelling masonry owing to its chaotic nature [38]. However, finite element models can overcome these challenges and accurately simulate the behaviour of masonry under seismic loading [39]. Additionally, finite element models can be used to analyse the response of reinforced masonry walls under axial compression, allowing for the prediction of buckling and failure modes [40]. Anisotropic constitutive models can be developed using detailed 3D continuum finite element representations to accurately capture the heterogeneous and anisotropic responses of masonry. Simple and refined models for masonry, including macroscopic models based on the assumption of no tension and refined models that account for the microscopic structure of masonry and interaction between blocks and interfaces, have been successfully used [41]. Different representations for studying regular masonry structures, including micromodelling, macromodelling, homogenisation, and structural component models, are well-known modelling strategies [21, 41-44].

## 2. Nonlinear analysis of masonry structures

The complex behaviour of masonry structures, particularly under seismic loading, requires using nonlinear analysis methods. Masonry exhibits highly nonlinear characteristics owing to its composite nature and the presence of joints, which act as a plane of weakness on the composite behaviour of masonry and can control the shear behaviour, particularly relevant in the case of strong unit–weak mortar joint combinations [45] and the brittle behaviour of its constituents.

Linear analysis methods, although simpler, often fail to capture crucial aspects of masonry behaviour, such as crack formation, progressive damage, and load redistribution, making the application of more sophisticated, nonlinear constitutive equations typically necessary; however, such constitutive equations require the acquisition of nonlinear material properties through various laboratory or in-situ mechanical tests [46]. Nonlinear analysis allows for a more accurate representation of the masonry behaviour throughout the entire loading process, from the initial elastic response to ultimate failure, particularly crucial for seismic analyses in which structures are subjected to cyclic loading and may experience significant deformations beyond the elastic limit [47]. The key aspects of nonlinear analysis of masonry structures include material, geometric, and contact nonlinearities.

Material nonlinearity accounts for the nonlinear stress–strain relationships of masonry components, including tension softening, compression hardening and softening, and shear behaviour [48]. Masonry units are a composite material with inherent nonlinear behaviour owing to their heterogeneous nature. The interaction between the mortar joints and masonry units leads to complex stress distributions and failure mechanisms. Nonlinear analysis can capture phenomena such as cracking and crushing of masonry units, sliding and opening of mortar joints, compressive softening, and tensile softening. For instance, Lourenço [44] developed a comprehensive continuum model for masonry that incorporated nonlinear material behaviours, providing a more accurate representation of the masonry response to loading.

Geometric nonlinearity is important for capturing large deformations and second-order effects, which can be significant in slender masonry structures [49, 50]. Masonry structures undergo large deformations, particularly during seismic events, and their geometries change significantly, which can result in P-delta effects and other geometric nonlinearities, affecting the overall structural response. Nonlinear analysis can account for these effects, particularly important when investigating slender structures or structures with irregular geometries [51].

Contact nonlinearity is essential for modelling the interactions between masonry units, particularly in dry-joint masonry or when considering crack formation and propagation [52]. Masonry structures often rely on friction and contact between elements for stability. Nonlinear analysis facilitates modelling these interactions, including the sliding between blocks, opening and closing of joints, and rocking of structural elements.

Several constitutive models and modelling strategies for the nonlinear analysis of masonry are available, including:

- **Plasticity-based models:** These models incorporate the nonlinear behaviour of masonry by considering plastic deformations and typically employ yield criteria to define the onset of plastic behaviour. Commonly used models include the Drucker–Prager model, adapted for masonry to account for its pressure-dependent strength, and the Mohr–Coulomb model, which represents the frictional behaviour of mortar joints. Lourenço et al. [53] proposed a composite plasticity model that combined different yield surfaces for tension, compression, and shear.
- **Damage models** play a crucial role in capturing the progressive deterioration of material properties attributed to microcracking, thus effectively representing the softening behaviour observed in masonry. Isotropic damage models assume uniform damage in all directions, whereas anisotropic damage models account for directional variations, offering a more realistic representation of the masonry behaviour. Papa et al. [54] developed an anisotropic damage model for masonry structures.
- **Combined Plasticity–Damage models:** These models integrate both plastic deformations and material degradation, providing a more comprehensive representation of the masonry behaviour. Pelà et al. [48] proposed a plastic damage model for analysing masonry structures under cyclic loading.

- **Micro-modelling approaches** represent masonry components (units and mortar) separately, allowing for a detailed analysis of the local behaviour. Detailed micromodelling represents units and mortar with continuum elements and unit-mortar interfaces with discontinuous elements. Simplified micromodelling represents expanded units with continuum elements and mortar joints with interfacial elements. Lourenço and Rots [55] developed a comprehensive micromodelling strategy for masonry analysis.
- **Macro-modelling approaches** treat masonry as a homogeneous continuum suitable for large-scale analyses. Orthotropic models consider the directional properties of the masonry, whereas applying homogenisation techniques helps derive the equivalent continuum properties from the microstructure of the masonry. Zucchini and Lourenço [56] proposed a homogenisation model that considers the interaction between masonry components.

The choice of constitutive model depends on the scale of analysis, computational resources, and specific phenomena of interest. Micro-modelling approaches offer detailed insights into local behaviour but are computationally intensive. Macro-modelling approaches are more suitable for larger structures but may oversimplify some aspects of the masonry behaviour. Recent trends include the development of multiscale models that combine the advantages of micro and macro approaches. Additionally, there is a growing interest in models that can capture the time-dependent behaviour of masonry, including creep and long-term damage accumulation. Integrating these constitutive models with advanced numerical techniques, such as FEM or DEM, has significantly enhanced the ability to analyse complex masonry structures under various loading conditions, including seismic actions. Future research directions include improving the representation of cyclic behaviour, developing more efficient computational algorithms, and incorporating uncertainties in the material properties and structural geometry. In this study, we employed a nonlinear finite element approach using a 2D simplified micro-modelling strategy. This method offers a lower level of detail than 3D modelling, particularly concerning the wall and joint thickness, but allows for the explicit representation of brick-and-mortar joints, capturing the nonlinear behaviour at the material level. The total strain rotating crack model used for bricks and the combined cracking-shearing-crushing model for joints enable a comprehensive representation of the various failure modes observed in masonry [53]. Furthermore, nonlinear analysis is crucial for evaluating strengthening techniques because it allows the assessment of structural performance beyond the elastic limit—particularly relevant for this current study on joint repointing, where the altered behaviour of strengthened joints can significantly impact the overall structural response.

By adopting a nonlinear approach, we aimed to capture the complex failure mechanisms, load redistribution, and ultimate capacity of masonry structures more accurately. This approach provides a better understanding of the structural behaviour and

**Table 1. Comparison of mechanical properties between unreinforced masonry (URM) and strengthened masonry (SM) specimens**

Property	URM	SM	Change
Compressive strength ( $f_c$ )	2.56 N/mm <sup>2</sup>	3.17 N/mm <sup>2</sup>	+24 %
Young's modulus (E)	1059.0 N/mm <sup>2</sup>	1145.3 N/mm <sup>2</sup>	+8 %
Ultimate strain (Compression)	0.0130	0.0443	+241 %
Diagonal tensile strength	0.1012 N/mm <sup>2</sup>	0.316 N/mm <sup>2</sup>	+212 %
Ultimate drift (Diagonal Compression)	0.308 %	0.252 %	-18 %
Modulus of rigidity (at 5 % max shear stress)	2323.99 N/mm <sup>2</sup>	5109.15 N/mm <sup>2</sup>	+120 %
Modulus of rigidity (at 30 % max shear stress)	1736.89 N/mm <sup>2</sup>	1532.40 N/mm <sup>2</sup>	-12 %
Modulus of rigidity (at 70 % max shear stress)	734.98 N/mm <sup>2</sup>	822.32 N/mm <sup>2</sup>	+12 %

enables a more reliable assessment and design of strengthening interventions for existing masonry buildings in seismic-prone areas.

### 3. Summary of experimental results

This study utilises experimental results from previous research [35] as a foundation for exploring the nonlinear finite element modelling of masonry walls subjected to compressive and diagonal compressive loads. This study focuses on the effectiveness of joint repointing as a method for strengthening masonry structures, with experimental investigations conducted on unreinforced and strengthened masonry panels using cement-polymer mortar and polypropylene strips in the bed joints, aiming to simulate the masonry in old buildings and test the effects of strengthening wall panels with structural joint repointing. The goal of this study is to develop a new repointing mortar with properties adjusted to match those of the units.

In this study, the term "old buildings" refers to structures constructed more than 50 years ago, primarily built with unreinforced masonry (URM) and lime-based mortar joints, predating modern seismic design codes and lacking contemporary structural reinforcement systems. These buildings, often of historical or cultural significance, are typically more vulnerable to seismic events owing to their construction methods and materials, thus making them the focus of our research on structural joint repointing as a method to enhance their seismic performance while preserving their historical integrity.

The experimental program consisted of in-plane and diagonal compressive tests on two groups of masonry panels: URM and strengthened masonry (SM). As a strengthening technique, the SM panels were reinforced using cement-polymer-based repointing mortar and polypropylene strips in the mortar joints. The specimens for both the axial and diagonal compression tests—designated as W-AP and W-DP for URM and WS-AP-RPP and WS-DP-RPP for SM—were constructed from solid clay bricks and lime mortar with fully filled head and bed joints. This targeted approach allowed for a focused comparison between the performances of URM and SM under specific loading conditions. More detailed information regarding the

experimental program, including specimen preparation, testing procedures, and full results, can be found in a prior study [35].

The experimental results demonstrated significant changes in the mechanical properties of masonry structures following the application of joint repointing with high-strength fibre-reinforced cement-polymer-based mortar and polypropylene strips. Table 1 presents a comparative overview of the key mechanical properties of URM and SM specimens. The data included both compressive and diagonal tensile loading scenarios, thereby providing insights into the complex impact of the strengthening technique. The values reported in Table 1 are the mean values derived from multiple test specimens. Notably, although these results show clear trends, the limited sample size should be considered when interpreting the data. Nonetheless, the consistent pattern of improvement across multiple parameters suggests a robust positive effect of the strengthening technique on the masonry performance.

As presented in Table 1, the joint repointing technique resulted in considerable improvements in strength but no improvement in the deformation capacity. Notably, the compressive strength increased by 24 %, whereas the diagonal tensile strength increased remarkably by 212 %. The tensile strength-to-compressive strength ratios for the URM and SM panels are 0.04 and 0.1, respectively. Lourenço and Gaetani [43] reported that the tensile strength for masonry ranges from  $(0.03 - 0.16) f_c$  for compressive strength in the range of 1–100 N/mm<sup>2</sup>. However, high-strength materials require further investigation because they are more brittle than low-strength materials.

The deformation capacity under compression, as indicated by the ultimate strain, exhibited a significant enhancement of 241 %. However, the ultimate drift under diagonal compression slightly decreased, suggesting a potential trade-off between strength and ductility. The results indicated that structural joint repointing significantly improved the strength of masonry, particularly when the original mortar exhibited low-strength properties. The test results provide valuable data for this study.

### 4. Modelling strategy and material model

Four main categories of modelling approaches for masonry and masonry structures based on different analysis approaches,

scales of material testing, and desired levels of accuracy and simplicity have been proposed: block-based models, continuum models, macro element models, and geometry-based models [42].

Three modelling strategies are commonly used: detailed micro-modelling, simplified micro-modelling, and macro-modelling [43, 44]. This study used a simplified micro-modelling approach (block-based model) (Figure 1). In the case of brick masonry, the location of potential cracks can be determined in advance; therefore, this strategy appears feasible for the simulation of experimental tests. However, for practical applications in engineering practice, smeared models or macro-modelling strategies seem to be preferable owing to their simplicity and reasonable and accurate prediction of the in-plane and out-of-plane behaviours of masonry walls [43, 57, 58]. The applied modelling methodology uses the FEM and a parameter-fitted nonlinear model to simulate and validate the experimental results in terms of load-deformation curves and damage patterns.

#### 4.1. Material model for simplified micro-model (SMM)

2D simplified micromodel was developed using the DIANA Finite Element Analysis software package [59]. Solid clay bricks were expanded in size by half-mortar thickness in both directions and were represented by continuum elements. The responses of the joints and brick-joint interface are lumped in zero-thickness interface discontinuous elements. This modelling approach considers material nonlinearities in both units and interfaces. All the failure modes were concentrated at the unit, bed, and head joint interfaces. To account for possible crack occurrences within the bricks and reproduce the crack progress from one head joint to the other, the brick units were divided into two halves by introducing a zero-thickness interface element, as shown in Figures 1 and 2.

The brick units were modelled using a constitutive nonlinear model based on the total strain crack model developed along the lines of the modified compression field theory originally proposed by Vecchio and Collins [60].

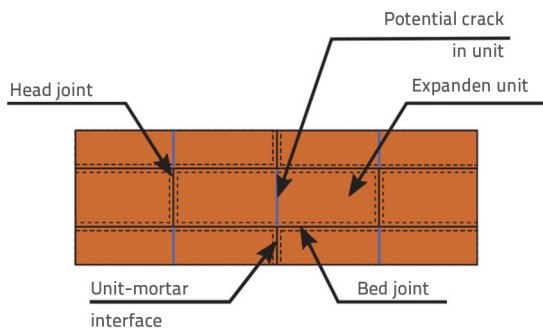


Figure 1. Implemented modelling strategy (adapted from [43])

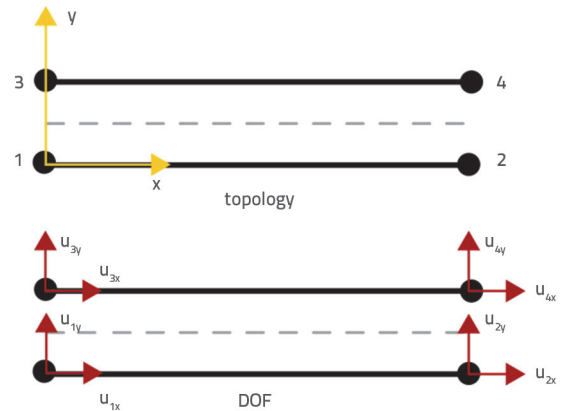


Figure 2. LBIF Interface element (adapted from [59])

A total-strain rotating crack model was used in this study. In the rotating crack model, shear softening occurs implicitly because of principal stress and strain coaxiality. The tensile behaviour is represented by an exponential tension-softening curve, as shown in Figure 3.a. In contrast, a parabolic stress-strain relationship was used to model the compressive behaviour, as shown in Figure 3.b. The tensile behaviour is directly related to the fracture energy in tension,  $G_{ft}^I$ , and characteristic element length  $h$ . The fracture energy of Mode I denotes the quantity of energy required to generate a unit area of a fully developed crack. During compression, the fracture energy  $G_c$  and characteristic element length  $h$  govern the softening part of the curve. A damage-based model was used for the Poisson's ratio reduction, and no reduction or increase in compressive strength owing to lateral confinement or cracking was used. The details of the implemented models can be found in the software documentation [59].

The composite interface model, also known as the combined cracking-shearing-crushing model, was used to model the brick-mortar interfaces. This model is suitable for modelling cracks, frictional slips, and crushing along material interfaces such as bed and head joints. A plane stress interface model formulated by Lourenço and Rots [61] and enhanced by Van Zijl [62] based on multisurface plasticity, which combines the Coulomb friction model with a tension cutoff and an elliptical compression cap, was used, as shown in Figure 4.

For the tensile and compressive modes, the associated flow rules were assumed, whereas a non-associated flow was commonly adopted for the shear mode. The schematic diagram depicts the evolution of three failure surfaces: the straight tension cut-off for Mode I failure, the Mohr-Coulomb friction law for Mode II failure, and the elliptical cap mode for shear-compression interaction. In addition, the figure shows that the three individual failure surfaces progress from the initial or maximum intermediate to the residual envelope.

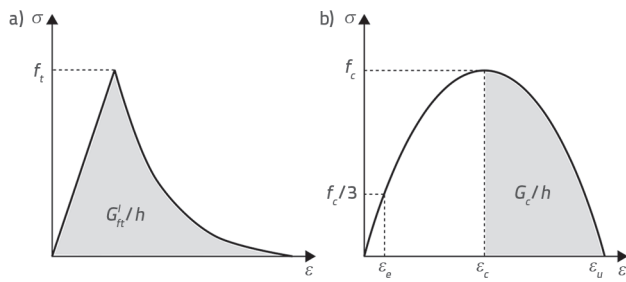


Figure 3. Tensile and compressive behaviour in total strain crack model (adapted from [59]): a) Exponential tension curve; b) Parabolic compression curve

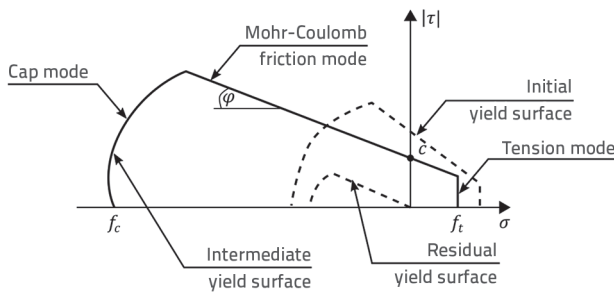


Figure 4. Two-dimensional interface model (adapted from [59])

During the analysis, the tensile strength, cohesion, and friction angle decreased (softening), whereas the compressive strength increased before decreasing (hardening-softening). For the tensile and compressive modes, the associated flow rules were assumed, whereas a non-associated flow was commonly adopted for the shear mode.

### 4.2. Implementation of the modelling strategy

The solid clay bricks were extended from dimensions of 250 × 120 × 60 mm<sup>3</sup> to 260 × 120 × 70 mm<sup>3</sup> to account for the mortar thickness (assumed to be 10 mm). The bricks were modelled with regular plane stress quadrilateral 4-noded finite elements (Q8MEM), and the bed and head joint interfaces were represented by structural line interface elements (L8IF) with 2+2 nodes. These elements characterise the behaviour of the interface in terms of the relationship between the normal and shear tractions, as well as the normal and shear relative displacements across the interface. In the 2D configuration, the interface element is located between two lines with a local-axis topology and two degrees of freedom per node, as shown in Figure 2. Thus, the mortar joints were modelled with zero thickness. The same type of structural line interface element was used to account for the possible cracking in the bricks; these elements connected the two halves of each brick. PP strips were included in the joint-repointed models using embedded

bar reinforcements. These reinforcements are embedded in structural (mother) elements and do not contribute to their mass or stiffness. In addition, the embedded reinforcements do not have their own degrees of freedom. The strains in the reinforcements were computed from the displacement fields of the mother elements, which ensured a perfect bond between the reinforcement and the surrounding material. However, the reinforcements influenced the stiffness of the mother elements. In this study, the embedded bar reinforcements were located at the bed-joint interfaces. Therefore, the stiffnesses in the normal,  $k_n$ , and shear directions,  $k_s$  and  $k_t$ , were computed using the free length of the interface as follows:

$$k_n = \frac{E}{l_{fr}}, \quad k_s = k_t = \frac{E}{2l_{fr}} \tag{1}$$

Where  $E$  is the Young’s modulus of the reinforcement bar and  $l_{fr}$  is the free length of the interface. In this case, zero thickness interface was applied, and therefore a virtual thickness of  $10^{-5}$  × distance from the first and second node of the interface element was assumed.

The PP strips were modelled using a linear elastic-perfectly plastic material model with the Von Mises yield condition, Young’s modulus of 2000 N/mm<sup>2</sup>, and yield stress of 150 N/mm<sup>2</sup> without plastic hardening. These parameters were adopted according to the manufacturer’s instructions [35].

The boundary conditions were modelled by restraining the translations of the bottom edges of the units in both orthogonal directions. The transfer steel elements positioned on top of the experimentally tested walls were not included in the developed models because their contact effect and friction were considered to have negligible effects on the load transfer from the actuators to the walls themselves.

The load was applied incrementally to the tops of the walls in small displacement increments until the ultimate displacement was reached. Therefore, the vertically restrained nodes at the top of the walls were selected as reference nodes for applying the prescribed displacements. The prescribed deformation 0.01 mm was used as the load-step increment.

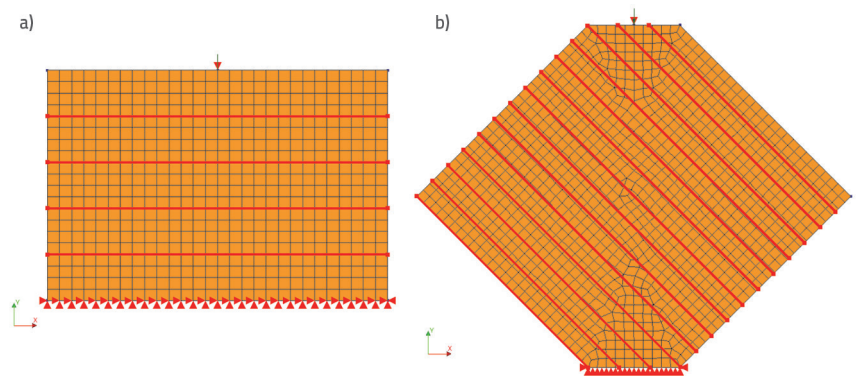


Figure 5. FE models of SM specimen for simulation of experimental tests: a) Configuration for compressive strength; b) Configuration for diagonal tensile strength test

Table 2. Average material properties for solid clay bricks, lime, and repointing mortar

Material	Length [mm]	Width [mm]	Height [mm]	Density [kg/m <sup>3</sup> ]	Compressive strength [N/mm <sup>2</sup> ]	Tensile flexural strength [N/mm <sup>2</sup> ]
<b>Solid clay brick</b>	249.8	122.8	57.8	1977.0	10.64	3.04
CoV [%]	--	--	--	1.0	19.7	19.3
<b>Lime mortar</b>	159.4	40.0	39.8	1650.2	0.94	0.73
CoV [%]	--	--	--	1.9	5.4	9.3
<b>Repointing mortar</b>	159.6	39.9	39.8	2200.1	32.86	12.0
CoV [%]	--	--	--	2.3	4.5	7.8

Table 3. Synthesis of input parameters for modelling the bricks and brick cracking in the middle

Bricks: Total strain-based crack model (TSBC)							
Young's modulus $E_b$ [N/mm <sup>2</sup> ]	Poisson's ratio $\nu_b$ [-]	Density $\rho$ [kg/m <sup>3</sup> ]	Tensile strength $f_t$ [N/mm <sup>2</sup> ]	Compressive strength $f_c$ [N/mm <sup>2</sup> ]	Mode-I frac. energy $G'_{ft}$ [N/mm]	Compressive frac. energy $G_c$ [N/mm]	Crack band
6,384	0.15	2·10 <sup>-9</sup>	1.0	10.64	0.072	16.5	Rots
Brick cracks: Discrete cracking							
Normal stiffness $k_n$ [N/mm <sup>3</sup> ]	Shear stiffness $k_t$ [N/mm <sup>3</sup> ]	Tensile strength $f_t$ [N/mm <sup>2</sup> ]	Mode-1 tension softening criterion	Fracture energy $G'_{ft}$ [N/mm]	Mode-II shear criterion for crack development		
1·10 <sup>6</sup>	1·10 <sup>6</sup>	1.0	Hordijk	0.01	Zero shear traction		

Table 4. Synthesis of input parameters for modelling the brick–joint interface

Combined cracking-shearing-crushing model							
Normal stiffness $k_n$ [N/mm <sup>3</sup> ]	Shear stiffness $k_t$ [N/mm <sup>3</sup> ]	Tensile strength $f_t$ [N/mm <sup>2</sup> ]	Tensile fracture energy $G'_{ft}$ [N/mm]	Cohesion $c$ [N/mm <sup>2</sup> ]	Friction angle $\mu$ [rad]	Dilatancy angle $\Psi$ [rad]	Res. friction angle [rad]
120 [200.0]	60 [80.0]	0.04 [0.14]	0.01 [0.08]	0.05 [0.15]	0.523599	0.349066	0.523599
Confining normal stress [N/mm <sup>2</sup> ]	Exponential degradation coefficient	Mode-II fracture energy $G'_s$ [N/mm]		Compressive strength $f_c$ [N/mm <sup>2</sup> ]	Compressive fracture energy $G_c$ [N/mm]	Shear traction factor $C_s$	Eq. plastic relat. displacement $\kappa_p$
		Par. (a)	Par. (b)				
-1.0	5	-0.01 [0.8]	0.009 [0.09]	2.77 [3.2]	6.25 [35]	9	0.01

A relatively dense finite element mesh was implemented by assigning an element size of 20 mm. The finite element models are presented in Figure 5. The additional steel elements used in the experiments were ignored in the FE models because of their negligible weight effects. Self-weight was considered the starting load. To ensure that the top wall edges were loaded uniformly, tying sets that created equal linear dependencies between the nodes in the FE mesh were used. Nonlinear structural analysis, considering physical and geometrical nonlinear effects, was performed using the default effect settings. A quasi-Newton (secant) method with BFGS iterations was used. The displacement convergence norm controls the iteration process with a convergence tolerance of 0.01.

Arch length control with default settings was used to predict displacement increments.

Due to the limited data obtained from the experimental tests, the material parameters required for the simulations were derived by combining the values obtained from the experimental tests and calibrating the parameters required for the material model used. The compressive strength, tensile flexural strength, and density of the bricks and mortars presented in Table 2 were obtained from experimental results [35].

The relationships given by Muhita et al. [16] and Lourenço and Gaetani [43] were used to relate the values of the other material parameters required for the nonlinear material models used. Tables 3 and 4 present the input parameters of the bricks

and structural interfaces for the URM specimen; the values in parentheses are valid for the SM specimen.

In the absence of test results, the modulus of elasticity of the bricks can be related to their compressive strength,  $f_c$ , and can be taken as  $(200-1000)f_c$ , depending on the material and load direction [43, 63], and in this simulation, it was adopted as  $600f_c$ . The compressive fracture energy was calculated using Eq. (2). The Poisson's ratio varies between 0.15 and 0.25, and the lowest value in the range was chosen.

The axial tensile strength  $f_t$  was not explicitly tested, and the value of the tensile flexural strength  $f_{ft}$  was obtained experimentally. According to Eq. (3) [43], the brick height,  $h_b$ , was used to determine the relationship between flexural and tensile strength, yielding a value of  $0.15f_c$ . Considering that the recommended values of  $f_t$  ranges from  $(0.03-0.12)f_c$  [43, 64], a value of  $0.1f_c$  was adopted. The fracture energy in tension,  $G_{ft}'$ , was calculated based on the brick compressive strength using Eqs. (4).

A combined cracking–shear–crushing model was used for the expanded joints. The required mechanical properties of the interface have been subjected to numerous attempts to calibrate the calculated results. However, the range of values is consistent with the recommendations of Lourenço and Gaetani [43]. The values calculated using the proposed equations were used as the approximate values to fit the results. To reproduce the crack progression from one head joint to another, a certain continuity between the head joints and vertical cracks in the bricks was assumed.

To avoid interpenetration, the two halves of the bricks were connected by interface elements with dummy normal and shear stiffnesses of  $10^6$  N/mm<sup>3</sup>.

$$G_c = \frac{32f_c}{10 + f_c} \tag{2}$$

$$f_t = \frac{0.06h_b^{0.7}}{1 + 0.06h_b^{0.7}} f_{ft} \tag{3}$$

$$G_{ft}' = 0.07 \ln(1 + 0.17f_c) \tag{4}$$

### 5. Results and discussion

Due to the limited data obtained from the experimental tests, the material parameters required for the simulations were derived by combining the values obtained from the experimental tests and calibrating the parameters required for the material model used. The compressive strength, tensile flexural strength, and density of the bricks and mortars presented in Table 2 were obtained from experimental results [35]. Tables 3 and 4 present the results of extensive testing and calibration of the developed FE model with respect to the experimental force–displacement curves and failure mechanisms. The calculated results were compared with the experimental results to determine the best parameter fit. The results were compared by inspecting the average experimental force–displacement curves in relation to the calculated force–displacement curves.

#### 5.1. Compressive strength

Figure 6 shows a comparison of the force–displacement curves for the URM and SM specimens obtained from experimental testing and numerical calculations (FEM-SMM). The targets of the finite element modelling and calibration of the material model were the average curves (AVG) and failure mechanisms. The linear elastic behaviour characterised in the range of 0–40 kN (for URM specimens) and 0–150 kN (for SM specimens) was well represented by the adopted modelling approach when compared to the average force–displacement curve. After

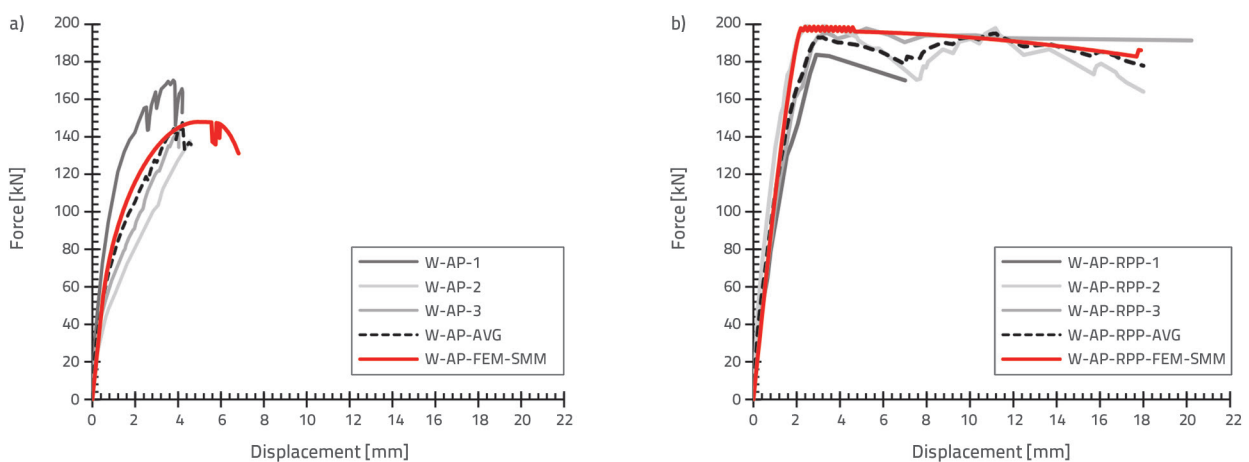


Figure 6. Comparison of experimental and numerical results for compressive strength: a) URM specimens ((W-AP-1÷3 = axial pressure for unreinforced walls, W-AP-AVG = average axial pressure, W-AP-FEM-SMM = FEM results for axial pressure, simplified-micro model)); b) SM specimens (WS-AP-RPP-1÷3 = axial pressure for strengthened walls, WS-AP-RPP-AVG = average axial pressure, WS-AP-RPP-FEM-SMM = FEM results for axial pressure, simplified-micro model)

Table 5. Comparison of experimental and FEM results for axial compression tests

Parameter	Unit	URM			SM		
		Experiment	FEM	Diff. [%]	Experiment	FEM	Diff. [%]
Load at first crack	kN	35.68	62.48	<b>54.6</b>	65.11	168.9	<b>88.7</b>
Displacement at first crack	mm	0.25	0.59	<b>81.0</b>	0.50	1.7	<b>109.1</b>
Initial stiffness	kN/mm	142.72	105.89	<b>-29.6</b>	130.22	99.35	<b>-26.9</b>
Peak load	kN	156.72	147.91	<b>-5.8</b>	194.32	198.68	<b>2.2</b>
Displacement at peak load	mm	4.2	4.96	<b>16.6</b>	10.8	2.59	<b>-122.6</b>
Compressive stress	N/mm <sup>2</sup>	2.56	2.42	<b>-5.6</b>	3.17	3.25	<b>2.5</b>
Ultimate displacement	mm	4.6	6.82	<b>38.9</b>	18.0	17.89	<b>-0.6</b>

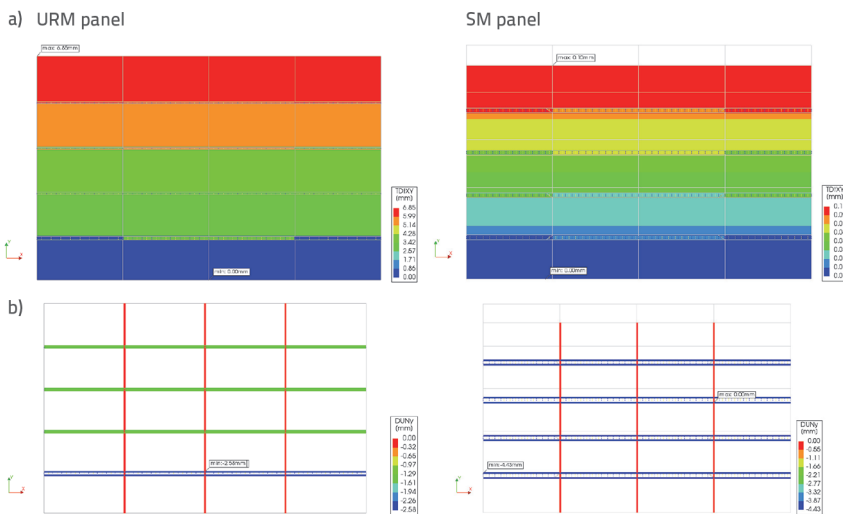


Figure 7. Numerical results from compression tests at the final calculation step (-cont.): a) Displacement field (mm); b) Interface relative displacement in vertical direction DUNY (mm)

the formation of the first cracks, the nonlinear behaviour was identified until a stable ultimate displacement was calculated. The peak force was approximated well, and for the URM specimens, the calculated ultimate displacements were larger than the experimentally obtained displacements.

After reaching the peak strength, a gradual softening behaviour was observed for the URM specimens, whereas for the SM specimens, the calculated behaviour exhibited almost perfectly plastic behaviour without any significant hardening or softening. A summary of the key results from both axial compression tests in terms of the averaged curve from the three tested walls in the unreinforced (URM, W-AP-AVG) and strengthened (SM, W-AP-RPP-AVG) cases and the corresponding FEM simulations are presented in Table 5.

The displacement field and interface relative displacement results for the ultimate load step for the compressive behaviour obtained for the URM and SM panels are shown in Figure 7. Owing to the vertical tying of all the nodes on the top edge of the wall and the dummy normal stiffness of the interface, no distinctive cracking pattern was observed in the bricks,

whereas the interfaces experienced relative vertical movement. As the load increased, the results showed a gradual increase in the interface displacements and tractions, resulting in crushing of the units and cracking at the interfaces, Figure 7.b, similar to the damage patterns obtained from the experimental tests. However, the experimental tests showed that a few cracks occurred in the bricks, and the FEM model was unable to capture this effect.

### 5.2. Diagonal tensile strength

Figure 8 shows a comparison of the force–displacement curves for both types of panels. The URM panels initially demonstrated an accurate simulated

elastic stiffness, subsequently compromised by the appearance of the first crack. Conversely, the SM panels slightly underestimated the initial stiffness values. The peak shear force was successfully simulated, with minor discrepancies in the displacements at the peak stress for the URM, which were slightly elevated, and the SM panel was closely correlated with the average experimental curves. Table 6 presents a summary of the key results, comparing the averaged curves from the three tested walls under diagonal compression for both the unreinforced (URM, W-AP-AVG) and strengthened (SM, W-AP-RPP-AVG) cases, along with the corresponding FEM simulation results.

The cracking patterns for both panels were reasonably well represented, as shown in Figure 9.a. In the URM panel, extensive cracking and sliding of the bed joints were observed; however, stair-step cracking along the bed and head joints appeared in the central part of the SM panel. This behaviour corresponded well with the damage obtained from the experimental tests, although diagonal sliding shear failure in the URM panel was not evident. Damage predominantly appeared at the bed joints of the URM and at the bed and head joints of the SM panel.

Table 6. Comparison of experimental and FEM results for diagonal compression tests

Parameter	Unit	URM			SM		
		Experiment	FEM	Diff. [%]	Experiment	FEM	Diff. [%]
Load at first crack	kN	8.64	9.74	12.0	15.67	35.49	77.5
Displacement at first crack	mm	0.04	0.05	22.2	0.05	0.16	104.8
Initial stiffness	kN/mm	216.0	194.8	-10.3	313.4	221.81	-34.2
Peak load	kN	16.64	17.64	5.8	53.59	53.06	-1.0
Displacement at peak load	mm	0.24	0.43	56.7	0.73	0.81	10.4
Shear stress	N/mm <sup>2</sup>	0.101	0.1	-1.0	0.316	0.301	-4.9
Ultimate displacement	mm	1.36	0.85	-46.2	1.20	1.03	-15.2

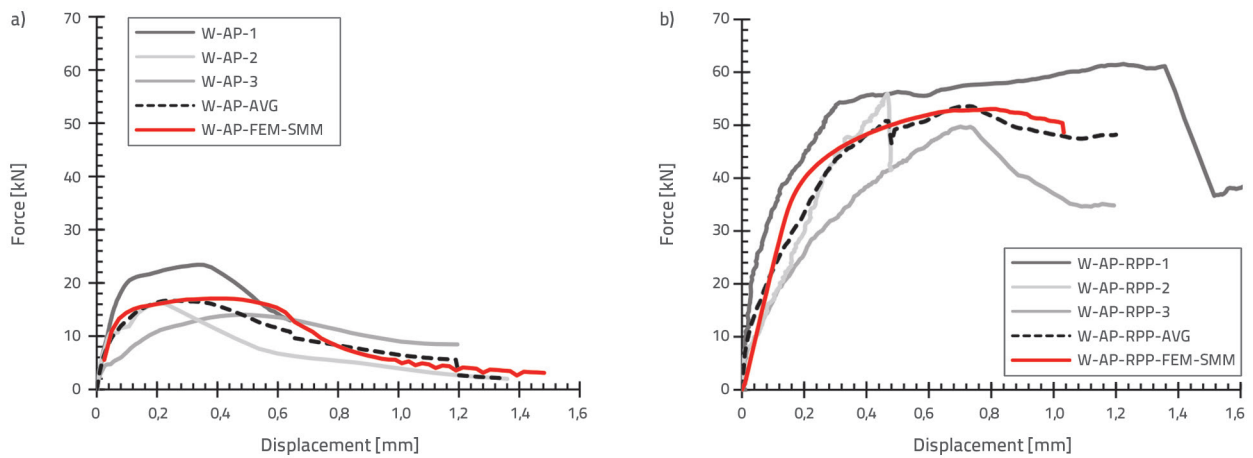


Figure 8. Comparison of experimental and numerical results for diagonal tensile strength: a) URM specimens (W-DP-1+3 = diagonal pressure for unreinforced walls, W-DP-AVG = average diagonal pressure, W-DP-FEM-SMM = FEM results for diagonal pressure, simplified-micro model); b) SM specimens (WS-DP-RPP-1+3 = diagonal pressure for strengthened walls, WS-DP-RPP-AVG = average diagonal pressure, WS-DP-RPP-FEM-SMM = FEM results for diagonal pressure, simplified-micro model)

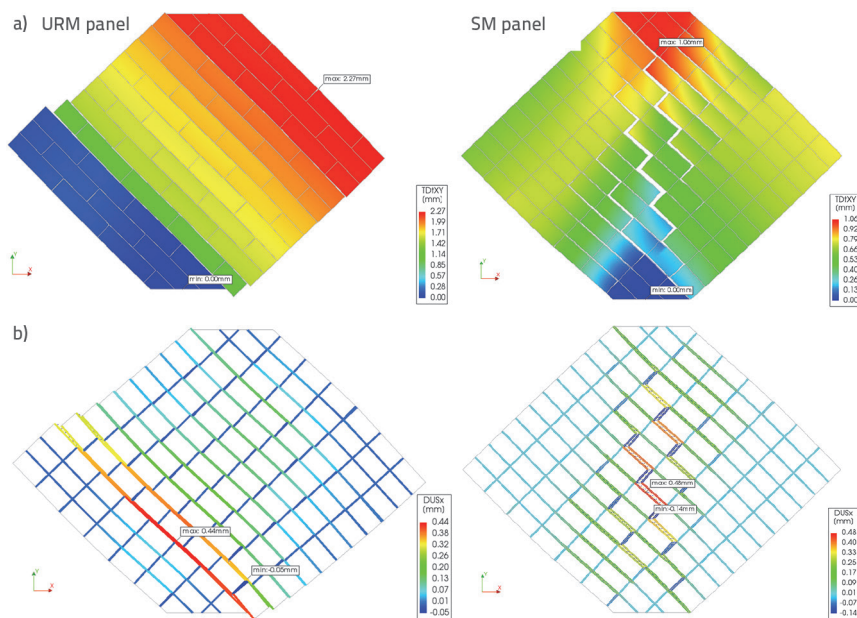


Figure 10. Numerical results at the final calculation step: a) Displacement field (mm); b) Interface relative displacement in shear direction DUSx (mm)

The relative displacements of the interface in the shear direction are shown in Figure 9.b. As expected, the stresses in the PP strips modelled as embedded reinforcements were quite low and well below their yielding stress.

Figure 10 shows the relevant total Cauchy stresses for both panels loaded under compression and diagonal tension. All PP strips experienced a very low tensile stress of approximately 1 N/mm<sup>2</sup>. For the SM panel, only a few locations along the vertical staircase crack generated stress with a maximum of 13.5 N/mm<sup>2</sup>. As a result of to these low stresses, the PP strips did not contribute to the overall compressive or diagonal tensile capacities of the tested panels, possibly because the PP strips were free to move in the bed joints without being constrained to the

walls. Owing to the strength properties of the mortar used for the joint repointing of the masonry, the overall capacity of the panel increased in both loading situations.

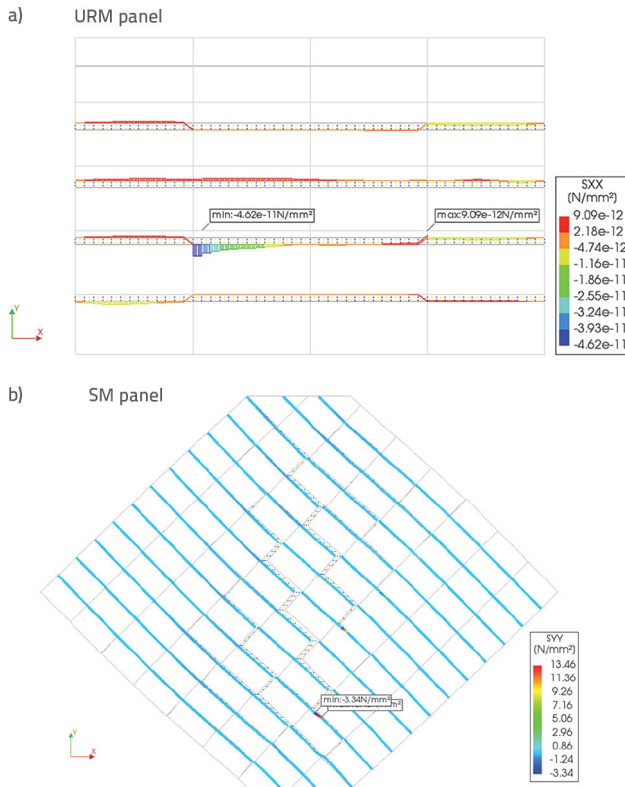


Figure 10. Relevant Cauchy total stresses in PP strips

## 6. Conclusions

This study demonstrated the application of finite element modelling and calibration in relation to experimental results. By utilising some of the input parameters obtained from the tests and calibrating the other required parameters for the material models, this study demonstrated the effectiveness of nonlinear calculations to accurately simulate the actual behaviour of brick walls, as evidenced by the close correlation between the numerical results and experimental data, thus validating the effectiveness of the modelling approach and material models for the analysis of brick masonry walls.

The simplified micro-modelling approach adopted in this research, which combines the total strain rotating crack model for bricks and the combined cracking-shearing-crushing model for joints, was proven highly effective in capturing the complex nonlinear behaviour of masonry, particularly evident in the simulations of the URM and SM panels under compressive and diagonal compressive loads.

For the compressive strength tests, the nonlinear finite element model effectively reproduced the overall experimental force–displacement curves for both URM and SM specimens. The FEM demonstrated high accuracy in predicting the peak loads and

compressive stresses, with differences within 6 % for both the URM and SM specimens, thus confirming the reliability of the model in estimating the ultimate strength parameters under axial compression. While the model accurately captured the onset of nonlinearity owing to crack formation and post-peak response, it significantly overestimated the load at the first crack (54.6 % for the URM and 88.7 % for the SM walls) and the displacement at the first crack (81.0 % for the URM and 109.1 % for the SM walls). These discrepancies suggest that the model requires improvement to capture cracking initiation, particularly for strengthened masonry under axial loads. For the URM, the FEM showed reasonable agreement in displacement prediction, overestimating the displacement at peak load by 16.6 % and ultimate displacement by 38.9 %. In contrast, for the SM, the FEM exhibited a significant underestimation of the displacement at the peak load (122.6 % lower) but excellent agreement for the ultimate displacement (0.6 % difference). These variations highlight the complexity of modelling masonry deformation under axial loads, particularly for strengthened specimens.

In the case of the diagonal tensile strength tests, the simulated force–displacement curves for both the URM and SM panels were consistent with the experimental results, particularly in capturing the peak forces, shear stress, and overall behaviour trends, with differences within 6 % for both the URM and SM specimens, thus demonstrating the effectiveness of the model in predicting the ultimate shear strength. The FEM simulation overestimates the load and displacement at the first crack to varying degrees, with load overestimations of 12.0 % for the URM and 77.5 % for the SM walls; the displacement overestimations are 22.2 % for the URM and 104.8 % for the SM walls. The larger discrepancies for the SM indicate that the model may require further refinement for strengthened masonry under diagonal compression. The FEM model overestimated the displacement at the peak load for both specimens: 56.7 % for the URM and 10.4 % for the SM walls. In contrast, the ultimate displacement was underestimated for both wall states: 46.2 % for URM and 15.2 % for SM walls. The ability of the model to represent the different failure mechanisms observed in URM and SM panels, extensive cracking and sliding in bed joints for URM, and stair-step cracking along the bed and head joints for SM further underscore its predictive capabilities. Overall, the numerical simulation demonstrated high reliability in predicting the peak loads and stresses for both the axial and diagonal compression tests. However, the model exhibited limitations, particularly at the onset of cracking and in the post-peak region. The discrepancies were generally more pronounced for the strengthened masonry specimens, suggesting that further refinement is required to accurately model the behaviour of strengthened systems. Moreover, nonlinear finite element analysis provides valuable insights into the stress distribution and failure mechanisms, which are difficult or impossible to observe directly in experiments. For instance, the model revealed the relative displacements at the interfaces and stress levels in the polypropylene strips used for strengthening, offering a

deeper understanding of the strengthening mechanism. By correctly predicting the behaviour of brick walls under various loading conditions, this nonlinear modelling approach serves as a powerful tool for assessing existing structures and designing effective strengthening interventions. Thus, this approach facilitates evaluating different strengthening strategies without requiring extensive and costly experimental programs, potentially leading to more efficient and economical solutions for preserving and enhancing masonry structures.

In conclusion, this study underscored the crucial role of nonlinear finite element modelling in bridging the gap between the theoretical understanding and actual structural behaviour of masonry. However, the models could be improved by determining the required material parameters through experimental tests instead of estimating values from the literature or by trial and error. These models can be beneficial if the values of the tensile

and bond strengths, cohesion, and mode I and II fracture energies are determined through testing.

## Acknowledgements

This study is based on the results of the Strengthening Masonry with Joint Repointing (STREP) project, realised with the cooperation of three partner institutions: the Faculty of Civil Engineering, Skopje, the Chair of Theory of Structures and Computational Analysis, and the Institute of Earthquake Engineering and Engineering Seismology, both parts of the Ss. Cyril and Methodius University in Skopje conducted the experimental tests and numerical simulations. ADING A.D. from Skopje was responsible for producing the specially modified joint repointing material and its application in the test models. We thank the laboratory staff for their technical assistance during this project.

## REFERENCES

- [1] Uroš, M., Šavor Novak, M., Atalić, J., Sigmund, Z., Baniček, M., Demšić, M., Hak, S.: Post-earthquake damage assessment of buildings – procedure for conducting building inspections, *GRAĐEVINAR*, 72 (2020) 12, pp. 1089-1115, <https://doi.org/10.14256/JCE.2969.2020>.
- [2] Radnić, J., Grgić, N., Buzov, A., Banović, I., Smilović Zulim, M., Baloević, G., Sunara, M.: Mw 6.4 Petrinja earthquake in Croatia: Main earthquake parameters, impact on buildings and recommendation for their structural strengthening, *GRAĐEVINAR*, 73 (2021) 11, pp. 1109-1128, <https://doi.org/10.14256/JCE.3243.2021>.
- [3] Šavor Novak, M., Uroš, M., Atalić, J., Herak, M., Demšić, M., Baniček, M., Lazarević, D., Bijelić, N., Crnogorac, M., Todorčić, M.: Zagreb earthquake of 22 March 2020 – preliminary report on seismologic aspects and damage to buildings, *GRAĐEVINAR*, 72 (2020) 10, pp. 843-867, <https://doi.org/10.14256/JCE.2966.2020>.
- [4] D'Altri, A.M., Cannizzaro, F., Petracca, M., Talledo, D.A.: Nonlinear modelling of the seismic response of masonry structures: Calibration strategies, *Bulletin of Earthquake Engineering*, 20 (2022), pp. 1999–2043, <https://10.1007/s10518-021-01104-1>.
- [5] Chang, L., Rots, J.G., Esposito, R.: Influence of aspect ratio and pre-compression on force capacity of unreinforced masonry walls in out-of-plane two-way bending, *Engineering Structures*, 249 (2021), <https://10.1016/j.engstruct.2021.113350>.
- [6] Di Re, P., Greco, M., Lofrano, E., Paolone, A.: Finite element modelling of masonry elements reinforced with the CAM system, *Structures*, 44 (2022), pp. 740-754, <https://doi.org/10.1016/j.istruc.2022.08.028>.
- [7] Chisari, C., Macorini, L., Izzuddin, B.A.: An anisotropic plastic-damage model for 3D nonlinear simulation of masonry structures, *International Journal for Numerical Methods in Engineering*, 13 (2022) 6, <https://doi.org/10.1002/nme.7162>
- [8] Ademović, N., Hrasnica, M.: Capacity degradation and crack pattern development in a multi-storey unreinforced masonry building, *GRAĐEVINAR*, 67 (2015) 4, pp. 351-361, <https://doi.org/10.14256/JCE.1191.2014>.
- [9] Cakir, F., Seker, B.S., Dogangun, A.: Assessment of structural performance of historical Ishan church, *GRAĐEVINAR*, 66 (2014) 5, pp. 433-443, <https://doi.org/10.14256/JCE.1015.2014>.
- [10] Boem, I.: Multi-layer modelling of masonry structures strengthened through textile-reinforced mortar [version 2; Peer review: 4 approved], *Open. Res. Europe* 2023, 2 (2023) 132, <https://doi.org/10.12688/openreseurope.15233.2>.
- [11] Boem, I.: Masonry elements strengthened with TRM: A Review of experimental, design and numerical methods, *Buildings*, 12 (2022) 9, p.1307, <https://doi.org/10.3390/buildings12091307>.
- [12] Hernoune, H., Benabed, B., Alshugaa, M., Abousnina, R., Guettala, A.: Strengthening of masonry walls with CFRP composite: experiments and numerical modelling, *Journal of Silicate Based and Composite Materials*, 2019., <https://doi.org/10.14382/epitoanyag-jsbcm.2020.1>.
- [13] Bernat-Maso, E., Gil, L., Roca, P.: Numerical analysis of the load-bearing capacity of brick masonry walls strengthened with textile reinforced mortar and subjected to eccentric compressive loading, *Engineering Structures*, 91 (2015), pp. 96-111, <https://doi.org/10.1016/j.engstruct.2015.02.032>.
- [14] Lignola, G.P., Prota, A., Manfredi, G.: Numerical investigation on the influence of FRP retrofit layout and geometry on the in-plane behavior of masonry walls, *Journal of composites for construction*, 16 (2012) 6, pp. 712-723, [10.1061/\(ASCE\)CC.1943-5614.0000297](https://doi.org/10.1061/(ASCE)CC.1943-5614.0000297).
- [15] D'Altri, A.M., Cannizzaro, F., Petracca, M., Talledo, D.A.: Nonlinear modelling of the seismic response of masonry structures: Calibration strategies, *Bulletin of Earthquake Engineering*, 20 (2022), pp. 1999–2043
- [16] Muhita, I.B., Masia, M.J., Stewart, M.G., Isfeld, A.C.: Spatial variability and stochastic finite element model of unreinforced masonry veneer wall system under Out-of-plane loading, *Engineering Structures*, 267 (2022).
- [17] Pari, M., Van de Graaf, A.V., Hendriks, M.A.N., Rots, J.G.: A multi-surface interface model for sequentially linear methods to analyse masonry structures, *Engineering Structures*, 238 (2021).

- [18] Chang, L., Rots, J.G., Esposito, R.: Influence of aspect ratio and pre-compression on force capacity of unreinforced masonry walls in out-of-plane two-way bending, *Engineering Structures*, 249 (2021).
- [19] Campbell, J., Silva, V., Balboa, R., Durán, M.: Numerical approach to determine the capacity curves of clay masonry walls with openings, *Rev. int. métodos numér. cálc. diseño ing*, 36 (2019) 1, p. 12
- [20] Vemuri, J., Ehteshamuddin, S., Ravula, M., Kolluru, S.: Pushover analysis of soft brick unreinforced masonry walls using analytical and numerical approaches, *Materials Today: Proceedings*, 28 (2020), Part 2, pp. 420-425
- [21] Medić, S.: Experimental and numerical analysis of solid brick masonry walls exposed to seismic loading, PhD thesis, Faculty of Civil Engineering, University of Sarajevo, Bosnia and Herzegovina, 2018.
- [22] Haach, V.G., Vasconcelos, G., Lourenço, P.B.: Study of the behaviour of reinforced masonry wallets subjected to diagonal compression through numerical modelling, *Proceedings of 9th International Masonry Conference in Guimarães, Portugal*, July 7-9, 2014.
- [23] Lemos, J.V., Sarhosis, V.: Discrete element bonded-block models for detailed analysis of masonry, *Infrastructures* 2022, 7 (2022) 3, p. 31, doi: <https://doi.org/10.3390/infrastructures7030031>.
- [24] Pulatsu, B., Gencer, F., Erdogmus, E.: Study of the effect of construction techniques on the seismic capacity of ancient dry-joint masonry towers through DEM, *European Journal of Environmental and Civil Engineering*, 26 (2020) 9, pp. 3913-3930, <https://doi.org/10.1080/19648189.2020.1824823>.
- [25] Masi, F., Stefanou, I., Maffi-Berthier, V., Vannucci, P.: A Discrete Element Method based-approach for arched masonry structures under blast loads, *Engineering Structures*, 216 (2020), p. 110721, <https://doi.org/10.1016/j.engstruct.2020.110721>.
- [26] Pulatsu, B., Bretas, E.M., Lourenço, P.B.: Discrete element modelling of masonry structures: Validation and application, *Universidade do Minho: RepositoriUM, Techno-Press*, 2016.
- [27] Sarhosis, V., Bagi, K., Lemos, J., Milani, G.: Computational modelling of masonry structures using the discrete element method, *IGI Global*, 2016.
- [28] Churilov, S., Dumova-Jovanoska, E.: Calibration of a numerical model for masonry with application to experimental results, *Architecture, Civil Engineering, Environment*, 3 (2008), pp. 41-48
- [29] Meguro K, Tagel-Din H.: Applied element method for structural analysis: Theory and application for linear materials, *Structural Engineering/Earthquake Engineering*, (2000).
- [30] Khattak, N., Derakhshan, H., Thambiratnam, D.P., Malomo, D., Perera, N.J.: Modelling the in-plane/out-of-plane interaction of brick and stone masonry structures using Applied Element Method, *Journal of Building Engineering*, 76 (2023), p. 107175, <https://doi.org/10.1016/j.jobe.2023.107175>.
- [31] Adhikari, R.K.; Parammal Vatter, A.; D'Ayala, D.: Seismic performance assessment of low-rise unreinforced and confined brick masonry school buildings using the Applied Element Method, *Buildings*, 13 (2023), p. 159. <https://doi.org/10.3390/buildings13010159>.
- [32] Sharma, S., Marasca, A., Ponte, M., Bento, R.: Modelling the in-plane cyclic behaviour of typical Portuguese rubble stone masonry using the applied element method, *Structures*, 46 (2022), pp. 1224-1242, doi: <https://doi.org/10.1016/j.istruc.2022.10.107>.
- [33] Adhikari, R., D'Ayala, D.: Applied Element Modelling and Pushover Analysis of unreinforced masonry buildings with flexible roof diaphragm, *Proceedings of the 7th International Conference on Computational Methods in Structural Dynamics and Earthquake Engineering, European Community on Computational Methods in Applied Sciences (ECCOMAS)*, 2019.
- [34] Malomo, D., Pinho, R., Penna, A.: Using the Applied Element Method for modelling calcium silicate brick masonry subjected to in-plane cyclic loading, *Earthquake Eng. Struct. Dyn.*, 47 (2018), pp. 1610-1630, <https://doi.org/10.1002/eqe.3032>.
- [35] Churilov, S., Dumova-Jovanoska, E., Shendova, V., Krstevska, L., Damchevski, B., Janchev, D.: Experimental investigation on masonry structural joint repointing with cement-polymer mortar and polypropylene strips, *GRAĐEVINAR*, 76 (2024) 7, pp. 607-620, <https://doi.org/10.14256/JCE.3893.2023>.
- [36] Tahat, H., Bedirhanoglu, I.: Finite Element Modelling of masonry wall retrofitted with combination of textile-reinforced mortar and thermal insulation, *Building for the Future: Durable, Sustainable, Resilient. fib Symposium 2023.- Lecture Notes in Civil Engineering*, 350 (2023), [https://doi.org/10.1007/978-3-031-32511-3\\_75](https://doi.org/10.1007/978-3-031-32511-3_75).
- [37] Di Re, P., Greco, M., Lofrano, E., Paolone, A.: Finite element modelling of masonry elements reinforced with the CAM system, *Structures*, 44 (2022), pp. 740-754, <https://doi.org/10.1016/j.istruc.2022.08.028>.
- [38] Brookes, C.L., Mehrkar-Asl, S.: Numerical modelling of masonry using discrete elements, *Seismic Design and Practice into the Next Century*, Routledge, 1998., doi: <https://www.doi.org/10.1201/9780203740026-18>.
- [39] Asad, M., Zahra, T., Thamboo, T., Song, M.: Finite element modelling of reinforced masonry walls under axial compression, *Engineering Structures*, 252 (2022), p. 113594, <https://doi.org/10.1016/j.engstruct.2021.113594>.
- [40] Chisari, C., Macorini, L., Izzuddin, B.A.: An anisotropic plastic-damage model for 3D nonlinear simulation of masonry structures, *International Journal for Numerical Methods in Engineering*, (2022), <https://doi.org/10.1002/nme.7162>.
- [41] Angelillo, M., Lourenço, P.B., Milani, G.: Masonry behaviour and modelling, *Mechanics of Masonry Structures*, CISM International Centre for Mechanical Sciences, 551 (2014).
- [42] D'Altri, A.M., Sarhosis, V., Milani, G.: Modelling strategies for the computational analysis of unreinforced masonry structures: Review and classification, *Archives of Computational Methods in Engineering*, 27 (2020), pp. 1153-1185, <https://doi.org/10.1007/s11831-019-09351-x>.
- [43] Lourenço, P.B., Gaetani, A.: Finite Element Analysis for building assessment: Advanced use and practical recommendations (1<sup>st</sup> ed.), *Routledge, Taylor & Francis Group*, 2022.
- [44] Lourenço, P.B.: Computational strategies for masonry structures, PhD dissertation, Delft University of Technology, 1996.
- [45] Vasconcelos, G.: Masonry Components, *Encyclopedia of Earthquake Engineering*, Springer, Berlin, Heidelberg, 2000., [https://doi.org/10.1007/978-3-642-35344-4\\_152](https://doi.org/10.1007/978-3-642-35344-4_152).
- [46] Roca, P., Cervera, M., Gariup, G., Pelà, L.: Structural Analysis of Masonry Historical Constructions: Classical and Advanced Approaches, *Arch. Computat. Methods Eng.*, 17 (2010), pp. 299-325, <https://doi.org/10.1007/s11831-010-9046-1>.
- [47] Asteris, P.G., Cavaleri, L., Di Trapani, F., Tsaris, A.K.: Numerical modelling of out-of-plane response of infilled frames: State of the art and future challenges for the equivalent strut macromodels, *Engineering Structures*, 132 (2017), pp. 110-122, <https://doi.org/10.1016/j.engstruct.2016.10.012>.

- [48] Pelà, L., Cervera, M., Roca, P.: An orthotropic damage model for the analysis of masonry structures, *Construction and Building Materials*, 41 (2013), pp. 957-967, <https://doi.org/10.1016/j.conbuildmat.2012.07.014>.
- [49] Addressi, D., Mastrandrea, A., Sacco, E.: An equilibrated macro-element for nonlinear analysis of masonry structures, *Engineering Structures*, 70 (2014), pp. 82-93, <https://doi.org/10.1016/j.engstruct.2014.03.034>.
- [50] Rizzano, G., Sabatino, R.: Non-linear static analysis of masonry structures by means of equivalent frames simplified approach, *Proceedings of the 8th International Masonry Conference, Dresden, Germany, 2010.*, pp. 1211-1220
- [51] Vrouva, A., Psycharis, I., Eleftheriou, V.: Parametric Investigation of the seismic response of ancient isodomic masonry walls, *Protection of Historical Constructions PROHITECH 2021, Lecture Notes in Civil Engineering*, 209 (2022), Springer, Cham, [https://doi.org/10.1007/978-3-030-90788-4\\_37](https://doi.org/10.1007/978-3-030-90788-4_37).
- [52] Mayorca, P., Meguro, K.: Modelling masonry structures using the Applied Element Method, *Journal of the Seisan - Kenkyu*, 56 (2003), pp. 581-584
- [53] Lourenço, P.B., Rots, J.G., Blaauwendraad, J.: Continuum model for masonry: Parameter estimation and validation, *Journal of structural engineering*, 124 (1998) 6, pp. 642-652, [https://doi.org/10.1061/\(ASCE\)0733-9445\(1998\)124:6\(642\)](https://doi.org/10.1061/(ASCE)0733-9445(1998)124:6(642)).
- [54] Papa, E.: A unilateral damage model for masonry based on a homogenisation procedure, *Mech. Cohes.-Frict. Mater.*, 1 (1996), pp. 349-366, [https://doi.org/10.1002/\(SICI\)1099-1484\(199610\)1:4<349::AID-CFM18>3.0.CO;2-M](https://doi.org/10.1002/(SICI)1099-1484(199610)1:4<349::AID-CFM18>3.0.CO;2-M).
- [55] Lourenço, P.B., Rots, J.G.: Multisurface interface model for analysis of masonry structures, *Journal of engineering mechanics*, 123 (1997) 7, pp. 660-668, [https://doi.org/10.1061/\(ASCE\)0733-9399\(1997\)123:7\(660\)](https://doi.org/10.1061/(ASCE)0733-9399(1997)123:7(660)).
- [56] Zucchini, A., Lourenço, P.B.: A micro-mechanical model for the homogenisation of masonry, *International Journal of Solids and Structures*, 39 (2002) 12, pp. 3233-3255, [https://doi.org/10.1016/S0020-7683\(02\)00230-5](https://doi.org/10.1016/S0020-7683(02)00230-5).
- [57] Milosević, J., Lopes, M., Gago, A.S. Bento, R.: Testing and modelling the diagonal tension strength of rubble stone masonry panels, *Engineering Structures*, 52 (2013), pp. 581-591
- [58] Sacco, E.: Micro, Multiscale and Macro Models for Masonry Structures, *Mechanics of Masonry Structures, CISM International Centre for Mechanical Sciences*, 551 (2014).
- [59] DIANA: DIANA Finite Element Analysis - User's Manual, Delft, The Netherlands, 2016.
- [60] Vecchio, F.J., Collins, M.P.: The modified compression field theory for reinforced concrete elements subjected to shear, *ACI Journal*, 83 (1986) 2, pp. 219-231
- [61] Lourenço, P.B., Rots, J.G.: A multi-surface interface model for the analysis of masonry structures, *Journal of Engineering Mechanics*, ASCE, 123 (1997) 7, pp. 660-668
- [62] Zijl, van, G.P. A.G.: Computational modelling of masonry creep and shrinkage, PhD thesis, Delft University of Technology, 2000.
- [63] Nowak, R., Kania, T., Derkach, V., Orłowicz, R., Halaliuk, A., Ekiert, E., Jaworski, R.: Strength parameters of clay brick walls with various directions of force, *Materials*, 14 (2021) 21, p. 6461
- [64] NZSEE: Seismic assessment of existing buildings (New Zealand Technical guidelines for engineering assessments) - Part C - Unreinforced masonry buildings, Wellington, New Zealand Society for Earthquake Engineering, 2017.